The Astrophysical Journal, 826:168 (9pp), 2016 August 1 doi:10.3847/0004-637X/826/2/168

GAS GIANT PLANET FORMATION IN THE PHOTOEVAPORATING DISK. I. GAP FORMATION

Lin Xiao[1], Liping Jin[2], Chengzhi Liu[1], and Cunbo Fan[1]
[1] Changchun Observatory, National Astronomical Observatories, CAS, Changchun, Jilin 130117, China; xiaol@cho.ac.cn
[2] College of Physics, Jilin University, Changchun, Jilin 130012, China
Received 2016 April 1; revised 2016 May 26; accepted 2016 May 27; published 2016 July 28

ABSTRACT

Planet formation and photoevaporation have both been considered as gap opening mechanisms in protoplanetary disks. We have studied giant planet formation in a photoevaporating disk with long-term evolution. Our calculations suggest that the core accretion rate of a protoplanet declines and the trigger of the runaway gas accretion for a giant planet is delayed under the action of photoevaporation. We find that the final mass of a giant planet characterized by the "gap-limiting" case is not influenced by photoevaporation but the final mass of a giant planet characterized by the "diffusion-limiting" case is greatly influenced by photoevaporation. Considering the formation process of giant planets, we suggest that the locations of the gaps opened by giant planets are within 30–40 au and the gap width in the "gap-limiting" case is wider than that in the "diffusion-limiting" case. We also find that gaps in photoevaporating disks are wider than those in non-photoevaporating disks. Our calculations suggest that the origins of multiple gaps in a disk can be diverse depending on their formation locations. In the formation region of giant planets, gaps are opened by giant planets. The outer gap beyond the giant planet formation region may be opened under the action of photoevaporation. A gap may also be opened at 1–3 au under the actions of photoevaporating dissipation and gas accretion of the outer giant planets.

Key words: planetary systems – planets and satellites: gaseous planets – protoplanetary disks

1. INTRODUCTION

Planets are born from protoplanetary disks. Observations of protoplanetary disks provide us with clues concerning the formation and evolution of planets (e.g., Williams & Cieza 2011; Isella et al. 2013; Akiyama et al. 2015; Ho 2016; van der Marel et al. 2016). Recently, ALMA Partnership et al. (2015) provided the first images of the protoplanetary disk around the young star HL Tauri (hereafter HL Tau) by observing the millimeter and submillimeter continuum emission with the Atacama Large Millimeter/submillimeter Array (ALMA). The images show that there are bright and dark rings in the disk of HL Tau. Hsi-Wei et al. (2016) also identify two HCO^+ gaps at radii of ∼28 and ∼69 au by analyzing the HCO^+ (1-0) data of HL Tau with ALMA.

A number of theoretical studies have been devoted to investigating the gap formation mechanism (e.g., Dong et al. 2015; Picogna & Kley 2015; Tamayo et al. 2015; Zhang et al. 2015; Akiyama et al. 2016; Jin et al. 2016; Yang et al. 2016). One hypothesis for the origin of gap structures is the planet–disk interaction (e.g., Lin & Papaloizou 1979; Goldreich & Tremaine 1980; Lin & Papaloizou 1993). Combining two-dimensional (2D) two-fluid hydrodynamic calculations with three-dimensional (3D) Monte Carlo Radiative Transfer simulations, Dong et al. (2015) suggest that multiple gaps can be opened by 0.2 M_J planets embedded in the disk. Dipierro et al. (2015) use the smoothed particle hydrodynamics code to simulate the global evolution of dust/gas disks with embedded multiple planets. They can reproduce the major features exhibited in HL Tau images with three embedded planets (0.2, 0.27, and 0.55 M_J) at 13.2, 32.3, and 68.8 au, respectively. Jin et al. (2016) adopt a method similar to that of Dong et al. (2015) to explore planet–disk interactions in the disk. They suggest that the masses of three embedded planets are about 0.35, 0.17, and 0.26 M_J, respectively. Recently, Akiyama et al. (2016) proposed that the observed features of multiple gaps in a disk may be the result of the combined effects of gravitational instability (GI) and type II migration.

Although the works mentioned above successfully reproduce the ring-like structures in protoplanetary disks, it is still uncertain whether all of the gaps in disks are opened by giant planets. The planet mass in a disk is usually set to a fixed value when 2D/3D hydrodynamical simulations of planet–disk interactions are performed (Dipierro et al. 2015; Dong et al. 2015; Jin et al. 2016). Since the formation and evolution of giant planets are not included, it is not clear whether planets can acquire sufficient masses to open deep gaps at given locations in disks. According to the core accretion model of giant planet formation (Pollack et al. 1996), it is very difficult to form giant planets outside 20–30 au in a protoplanetary disk (e.g., Ida & Lin 2004; Mordasini et al. 2009). Although GI may be another giant planet formation scenario, a disk becomes gravitationally unstable only in the outer region and the disk fragments are more likely to evolve into brown dwarfs or low-mass stars rather than planets (e.g., Rice et al. 2015; Kratter & Lodato 2016).

Both observations and theoretical models of protoplanetary disks confirm that disk dispersal is very efficient (e.g., Alexander et al. 2014; Espaillat et al. 2014). Photoevaporation may be the dominant mechanism that drives the dispersal of disks around classical and weak-lined T Tauri stars (Armitage 2011). Far-ultraviolet (FUV), extreme-ultraviolet (EUV), or X-ray radiation from the central star heat the disk surface (Font et al. 2004; Gorti et al. 2009; Owen et al. 2010). When the mass-loss rate due to photoevaporation by high-energy radiation at a given location in a disk is larger than the mass replenishment rate by viscous processes at that location, then a gap opens in the disk. The number and location of the gaps depend on the disk size and surface density profile (Morishima 2012; Bae et al. 2013; Rosotti et al. 2015; Xiao & Li 2016). Compared with the low mass-loss rate of EUV photoevaporation (Font et al. 2004), X-ray photoevaporation

can produce a much higher mass-loss rate due to its ability to penetrate (e.g., Gorti et al. 2009; Owen et al. 2010, 2011, 2012).

The goal of this study is to investigate giant planet formation in photoevaporating disks with long-term evolution. We further develop the disk model introduced in Xiao & Jin (2015) by taking into account X-ray photoevaporation (Gorti et al. 2009; Owen et al. 2010, 2011, 2012). To calculate the giant planet mass, we adopt the same models for planet growth as those in Xiao & Jin (2015) which are based on the core accretion scenario. This paper is organized as follows. In Section 2, we provide the details on our disk model and giant planet formation model. Our calculation results and discussions are presented in Section 3 and Section 4, respectively. Finally, our conclusions are presented in Section 5.

2. MODELS FOR DISK EVOLUTION AND GIANT PLANET FORMATION

We describe our one-dimensional (1D) viscous disk evolution model that includes mass infall from the progenitor cloud core onto the disk in Section 2.1. We recapitulate the long-term growth model of gas giant planets that includes solid core accretion, slow envelope accretion, runaway gas accretion, and gap opening in Section 2.2.

2.1. Disk Evolution Equations

Our disk model simulates the time evolution of the gas surface density of the disk, which is based on a numerical solution of the diffusion equation (Jin & Sui 2010). The mass infall rate onto the protoplanetary disk from its progenitor core is based on Cassen & Moosman (1981). According to Shu (1977), the properties of a cloud core are described by the core mass $M_{\rm cd}$, angular velocity ω, and temperature $T_{\rm cd}$. The observational ranges of ω and $T_{\rm cd}$ are 0.1–13 $\times$ 10^{-14} s^{-1} and 7–40 K, respectively (Goodman et al. 1993; Jijina et al. 1999; Caselli et al. 2002). In this study, we set the physical parameters with $M_{\rm cd} = 1.2\ M_\odot$, $\omega = 1 \times 10^{-14}$ s^{-1}, and $T_{\rm cd} = 15$ K to discuss the disk structures (e.g., Robitaille et al. 2007; Guilloteau et al. 2011; Kwon et al. 2011).

We update the disk model introduced in Jin & Sui (2010) and Xiao & Jin (2015) by considering X-ray photoevaporation (Gorti et al. 2009; Owen et al. 2010, 2011, 2012) and the accretion of giant planets. The diffusion equation of the disk surface density is

$$\frac{\partial \Sigma(R,t)}{\partial t} = \frac{3}{R}\frac{\partial}{\partial R}\left[R^{1/2}\frac{\partial}{\partial R}(\Sigma\nu R^{1/2})\right] + S(R,t) + S(R,t)\left\{2 - 3\left[\frac{R}{R_{\rm d}(t)}\right]^{1/2} + \frac{R/R_{\rm d}(t)}{1+[R/R_{\rm d}(t)]^{1/2}}\right\} - \dot{\Sigma}_{\rm w}(R) - \dot{Q}_{\rm planet}, \quad (1)$$

where Σ is the gas surface density of the disk, R is the cylindrical radius, ν is the kinematic viscosity, and $\dot{\Sigma}_{\rm w}(R)$ is the photoevaporation term. The mass influx $S(R,t)$ from the collapsing cloud core onto the disk is (Nakamoto & Nakagawa 1994)

$$S(R,t) = \begin{cases} \dfrac{\dot{M}_{\rm cd}}{4\pi R R_{\rm d}(t)}\left[1 - \dfrac{R}{R_{\rm d}(t)}\right]^{-1/2} & if\ \frac{R}{R_{\rm d}(t)} < 1; \\ 0 & \text{otherwise,} \end{cases} \quad (2)$$

where $\dot{M}_{\rm cd} = 0.975(\Re/\mu)^{3/2}T_{\rm cd}^{3/2}/G$ is the mass infall rate (Shu 1977). The centrifugal radius, $R_{\rm d}(t)$, is

$$R_{\rm d}(t) = 31\left(\frac{\omega}{10^{-14}\ {\rm s}^{-1}}\right)^2\left(\frac{T_{\rm cd}}{10\ {\rm K}}\right)^{1/2}\left(\frac{t}{5\times10^5\ {\rm yr}}\right)^3 {\rm au}. \quad (3)$$

We calculate the disk temperature with radiative diffusion approximation which is the same as that used in Jin & Sui (2010) and Xiao & Jin (2015). We use the α-prescription to calculate the kinematic viscosity (Shakura & Sunyaev 1973), $\nu = \alpha c_{\rm s} h$, where $c_{\rm s}$ is the sound speed, h is the half thickness of the disk, and α is a dimensionless parameter reflecting the viscosity strength which varies with both R and t:

$$\alpha = \max[\alpha_{\rm GI} + \alpha_{\rm MRI}, \alpha_{\rm min}], \quad (4)$$

where $\alpha_{\rm GI}$ is the viscosity parameter due to GI (Laughlin & Bodenheimer 1994; Laughlin & Rozyczka 1996; Laughlin et al. 1997, 1998), $\alpha_{\rm MRI}$ is the viscosity parameter of magnetorotational instability (MRI; Balbus & Hawley 1991, 1998), and $\alpha_{\rm min}$ is the minimum value for driving disk evolution. In this study, when a disk becomes gravitationally unstable, a spiral structure develops which is prone to stabilizing the disk and preventing disk fragmentation. We take $\alpha_{\rm GI} = (\alpha_{\rm short}^2 + \alpha_{\rm long}^2)^{1/2}$ according to Kratter et al. (2008), where $\alpha_{\rm short} = \max[0.14(1.3^2/Q^2 - 1)(1-u)^{1.15}, 0]$ and $\alpha_{\rm long} = \max[1.4\times10^{-3}(2-Q)/(u^{1.25}Q^{0.5}), 0]$, where Q is the Toomre parameter (Toomre 1964) and u is the ratio of the disk mass to the mass of protostar+disk. We set $\alpha_{\rm MRI}$ according to the numerical results of Fleming & Stone (2003), who consider the non-ideal magnetohydrodynamic (MHD) effects in their 3D layered disk models to explore local dynamics. In the region where GI and MRI cannot survive, the hydrodynamic effects may drive disk evolution. The viscosity caused by the hydrodynamics is still uncertain (e.g., Armitage 2011). Here, $\alpha_{\rm min}$ is taken to be constant, $\alpha_{\rm min} = 1.5\times10^{-3}$, which is the median value from Dubrulle (1993), Klahr & Bodenheimer (2003), and Chambers (2006a).

The sink term $\dot{Q}_{\rm planet}$ is the mass-loss rate of the disk due to gas accretion by the forming planets (Alibert et al. 2013). Photoevaporation induced by X-rays is simulated using radiation-hydrodynamic models (e.g., Ercolano et al. 2009; Owen et al. 2010, 2011, 2012). Owen et al. (2011, 2012) estimate the total mass-loss rate as follows:

$$\dot{M}_{\rm w} = 6.25\times10^{-9}\left(\frac{M_*}{1\ M_\odot}\right)^{-0.068} \times \left(\frac{L_{\rm X}}{10^{30}\ {\rm erg\ s}^{-1}}\right)^{1.14} M_\odot\ yr^{-1}, \quad (5)$$

where M_* is the central star mass and $L_{\rm X}$ is the X-ray luminosity. According to Bae et al. (2013), $L_{\rm X}$ is a function of

M_* for a low-mass star ($M_* \leqslant 2\ M_\odot$):

$$\log(L_X\,[\mathrm{erg\ s^{-1}}]) = 30.37(\pm 0.06) + 1.44(\pm 0.10)\log(M_*/M_\odot). \quad (6)$$

Owen et al. (2012) show that $\dot{\Sigma}_w(R) = A\dot{\Sigma}_{w,scale}$, and $\dot{\Sigma}_{w,scale}$ is presented in their Appendix B. The scale coefficient, A, is determined by

$$\dot{M}_w = A\int 2\pi R\dot{\Sigma}_{w,scale}\,dR \quad (.\ 7)$$

2.2. Giant Planet Formation Model

We adopt the core accretion model of giant planet formation used in Xiao & Jin (2015) to calculate giant planets' masses, which include protoplanetary solid core accretion and gas accretion (Pollack et al. 1996). Since the trapping of migrating planets in the protoplanetary disk is still an open issue (e.g., Masset & Papaloizou 2003; Pepliński et al. 2008; Paardekooper & Papaloizou 2009; Hasegawa & Pudritz 2011; Nayakshin 2015; Ogihara et al. 2015), we do not consider planet migration in this study. Moreover, the ring-like structures in disks imply that giant planets may form in situ (ALMA Partnership et al. 2015). We assume that giant planets locate at 13.1, 28.6, and 39.5 au, respectively.

2.2.1. Protoplanetary Solid Core Accretion

The calculations of the growth rate of a protoplanetary solid core are based on the oligarchic growth model by Chambers (2006b), who also considers the surface density evolution of planetesimals and fragments produced by collisions between planetesimals. The solid core accretion rate of an embedded protoplanet due to planetesimal accretion is written as

$$\frac{dM_c}{dt} = 36.5\frac{\Sigma_p\Omega r_h R_c}{\tilde{e}^2_{m,eq}}, \quad (8)$$

where M_c and R_c are the mass and the physical radius of a solid core, respectively, Σ_p is the surface density of planetesimals, Ω is the orbital angular velocity of the embedded protoplanet, and r_h is the protoplanet's Hill radius, which is

$$r_h = a\left(\frac{M_c}{3M_*}\right)^{1/3}, \quad (9)$$

where a is the orbital semimajor axis of the protoplanet and M_* is the central star mass. The equilibrium eccentricity, $\tilde{e}_{m,eq}$, is defined as

$$\tilde{e}_{m,eq} = 2.61\left(\frac{r}{5\ \mathrm{km}}\right)^{1/5}\left(\frac{\rho_p}{2\ \mathrm{g\ cm^{-3}}}\right)^{1/5}\left(\frac{b}{10}\right)^{-1/5}\left(\frac{C_D}{1}\right)^{-1/5} \times\left(\frac{\rho_{gas}}{2\times 10^{-9}\ \mathrm{g\ cm^{-3}}}\right)^{-1/5}\left(\frac{a}{1\ \mathrm{au}}\right)^{-1/5} \quad (10)$$

(see Kokubo & Ida 2002 and Thommes et al. 2003), where r is the physical radius of the planetesimals, ρ_p is the bulk density of the solid core, ρ_{gas} is the local gas density of the protoplanetary disk, C_D is the gas drag coefficient (Adachi et al. 1976), and the orbital separation b is measured in r_h. The typical value of b is ~10, which is independent of the disk and the protoplanet parameters (Kokubo & Ida 1998). The solid core accretion rate of an embedded protoplanet due to fragment accretion is

$$\frac{dM_c}{dt} = 11.3\Sigma_f\Omega r_h^{3/2}R^{1/2}, \quad (11)$$

where Σ_f is the surface density of fragments.

Chambers (2006b) considers solid material evolution in order to obtain self-consistent equations for the solid core accretion rate. He assumes that the total solid materials are composed of planetesimals, fragments, and solid cores of protoplanets in the protoplanetary disk:

$$\Sigma_{tot} = \Sigma_p + \Sigma_f + \Sigma_e, \quad (12)$$

where Σ_e is the equivalent surface density of a protoplanet solid core, which is given by

$$\Sigma_e = \frac{M_c}{2\pi abr_h}. \quad (13)$$

The decreasing rate of the planetesimal surface density due to mutual collisions is expressed as

$$\frac{d\Sigma_p}{dt} = -\frac{11.04\Omega\Sigma_p^2 r^2 f(Q_{col})}{m}, \quad (14)$$

where m is the mass of planetesimals, and

$$f(Q_{col}) = \begin{cases}\dfrac{Q_{col}}{2Q^*} & \text{if } Q_{col} < 2Q^*,\\ 1 & \text{if } Q_{col} \geqslant 2Q^*,\end{cases} \quad (15)$$

where Q_{col} is the collision energy per unit target mass

$$Q_{col} = \frac{5}{4}\Omega^2 r_h^2\tilde{e}^2_{m,eq}, \quad (16)$$

and Q^* is the mean catastrophic disruption threshold

$$Q^* = Q_0\left(\frac{r}{1\ \mathrm{cm}}\right)^a + B\rho_p\left(\frac{r}{1\ \mathrm{cm}}\right)^b, \quad (17)$$

where $Q_0 = 3.5\times 10^7\ \mathrm{erg\ g^{-1}}$, $B = 0.3\ \mathrm{erg\ cm^3\ g^{-2}}$, $a = -0.38$, and $b = 1.36$ (Benz & Asphaug 1999).

From the above equations, we derive the normalized surface densities, $\sigma = \Sigma_k/\Sigma_{tot}$ (k = p, f, e), and change rates (Xiao & Jin 2015)

$$\begin{aligned}\frac{d\sigma_e}{dt} &= A\sigma_p\sigma_e^{1/2} + B\sigma_f\sigma_e^{1/2},\\ \frac{d\sigma_p}{dt} &= -A\sigma_p\sigma_e^{1/2} - C,\\ \frac{d\sigma_f}{dt} &= -B\sigma_f\sigma_e^{1/2} + C,\end{aligned} \quad (18)$$

where

$$A = \frac{5.01}{b^{1/2}\tilde{e}_{\rm m,eq}^2}\left(\frac{\Omega\Sigma_{\rm tot}^{1/2}}{\rho_{\rm p}^{1/3}M_*^{1/6}}\right),$$

$$B = \frac{1.64}{b^{1/2}}\left(\frac{a^{1/2}\Omega\Sigma_{\rm tot}^{1/2}}{\rho_{\rm p}^{1/6}M_*^{1/3}}\right),$$

$$C = \begin{cases} 3.45b\tilde{e}_{\rm m,eq}^2\left(\dfrac{\Omega^3a^4\Sigma_{\rm tot}^2}{\rho_{\rm p}rM_*Q^*}\right)\sigma_{\rm p}^2\sigma_{\rm e} & \text{if } Q_{\rm col} < 2Q^*, \\ \dfrac{2.64\Omega\Sigma_{\rm tot}}{\rho_{\rm p}r}\sigma_{\rm p}^2 & \text{if } Q_{\rm col} \geqslant 2Q^*. \end{cases} \quad (19)$$

In this study, we adopt the same approach as in Xiao & Jin (2015) to set $\Sigma_{\rm tot}$ and the starting time of planet formation. The initial mass of the protoplanet, $M_{\rm ini}$, is set by

$$M_{\rm ini} = \left[\frac{\pi m\Sigma_{\rm tot}a^2b}{(3M_*)^{1/3}}\right]^{3/5}, \quad (20)$$

which is obtained from the condition for the transition from runaway to oligarchic growth of the protoplanet (Ida & Makino 1993).

2.2.2. Gas Accretion onto a Protoplanet

When the protoplanet mass is small, it accretes gas from the disk due to the contraction of the gaseous envelope which is characterized by slow gas accretion (Xiao & Jin 2015). According to Miguel & Brunini (2008) and Miguel et al. (2011), the gas accretion rate in this case is written as

$$\dot{M}_{\rm slow} = \frac{dM_{\rm g}}{dt} = \frac{M}{\tau_{\rm g}}, \quad (21)$$

where $M_{\rm g}$ is the gaseous envelope mass, M is the total mass of the protoplanet, and $\tau_{\rm g}$ is the characteristic growth time,

$$\tau_{\rm g} = 8.35 \times 10^{10}\left(\frac{M}{M_\oplus}\right)^{-4.89}\ {\rm yr}. \quad (22)$$

The classical formation models of giant planets show that when a planet is massive enough, the gas envelope cannot be in equilibrium and the runaway gas accretion is triggered (e.g., Pollack et al. 1996; Ikoma et al. 2000). According to Tanigawa & Ikoma (2007), the gas accretion afterward can be divided into two cases: the "diffusion-limiting" case (in which the gas accretion of the protoplanet is determined by the gas supply of the disk) and the "gap-limiting" case (in which the gas accretion of the protoplanet is determined by the gap opening in the disk). In the "gap-limiting" case, the gas accretion rate is written as (Tanigawa & Watanabe 2002)

$$\dot{M}_{\rm gap} = \frac{dM_{\rm g}}{dt} = \dot{A}\Sigma_{\rm acc}, \quad (23)$$

where

$$\dot{A} = 0.29\left(\frac{h}{a}\right)^{-2}\left(\frac{M}{M_*}\right)^{4/3}a^2\Omega \quad (24)$$

and $\Sigma_{\rm acc} = \Sigma_{\rm gap}(x = 2r_{\rm h})$. The equilibrium surface density profile, $\Sigma_{\rm gap}(x)$, which is considered to be the actual gas surface density of the protoplanetary disk around a protoplanet, is given by (Tanigawa & Ikoma 2007)

$$\Sigma_{\rm gap}(x) = \begin{cases} \Sigma(a,\,t)\exp\left[-\left(\dfrac{x}{l}\right)^{-3}\right] & \text{if } x > x_{\rm m}, \\ \Sigma(a,\,t)\exp\left[-\dfrac{1}{2}\left(\dfrac{x}{h} - \dfrac{5}{4}\dfrac{x_{\rm m}}{h}\right)^2 + \dfrac{1}{32}\left(\dfrac{x_{\rm m}}{h}\right)^2 - \left(\dfrac{x_{\rm m}}{l}\right)^{-3}\right] & \text{if } x \leqslant x_{\rm m}, \end{cases} \quad (25)$$

where x is the distance to the embedded planet on the line from the star through the planet, and l and $x_{\rm m}$ are defined as

$$l = 0.146\left(\frac{\nu}{10^{-5}a^2\Omega}\right)^{-1/3}\left(\frac{M}{10^{-3}M_*}\right)^{2/3}a, \quad (26)$$

$$x_{\rm m} = 0.207\left(\frac{h}{0.1a}\right)^{2/5}\left(\frac{\nu}{10^{-5}a^2\Omega}\right)^{-1/5}\left(\frac{M}{10^{-3}M_*}\right)^{2/5}a. \quad (27)$$

From the above, the gas accretion rate onto the protoplanet, $\dot{M}_{\rm g}$, is written as

$$\dot{M}_{\rm g} = \frac{dM_g}{dt} = \min(\dot{M}_{\rm slow},\,\dot{M}_{\rm gap},\,\dot{M}_{\rm disk}), \quad (28)$$

where $\dot{M}_{\rm disk}$ is the mass accretion rate of the disk (Jin & Sui 2010). It should be noted that $\dot{M}_{\rm g}$ equals the mass-loss rate of the disk due to gas accretion by the forming planets ($\dot{Q}_{\rm planet}$; Alibert et al. 2013).

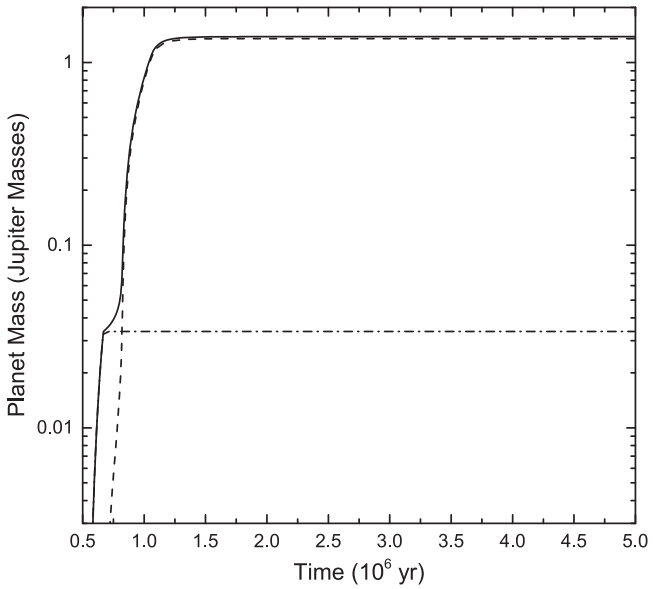

Figure 1. Time evolution of planetary mass at 13.1 au in the non-photoevaporating disk with $\omega = 1.0 \times 10^{-14}\ {\rm s}^{-1}$, $T_{\rm MCC} = 15$ K, and $M_{\rm MCC} = 1.2\,M_\oplus$. The solid lines represent total planet mass, the dashed lines accumulated gas mass, and the dot–dashed lines accumulated solid mass.

3. RESULTS

3.1. Planet Formation in the Non-photoevaporating Disk

In Figure 1, the planet is located at 13.1 au. As discussed by Xiao & Jin (2015), the surface densities of solids and gases in

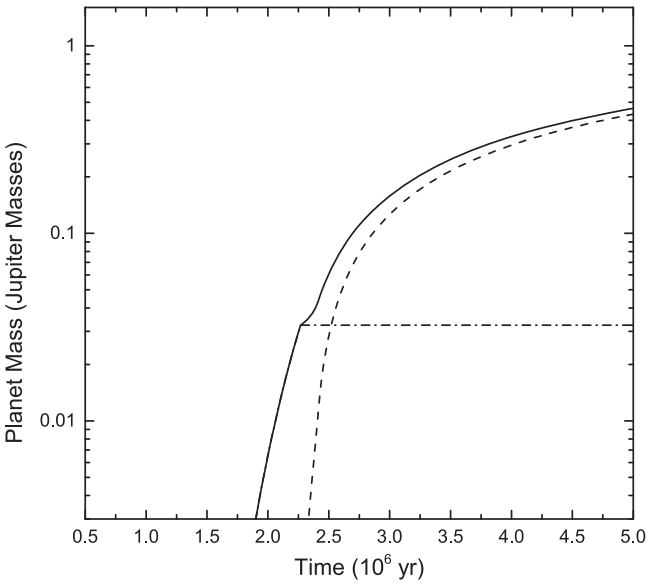

Figure 2. Time evolution of planetary mass at 28.6 au in the non-photoevaporating disk with $\omega = 1.0 \times 10^{-14}\,\mathrm{s}^{-1}$, $T_{\mathrm{MCC}} = 15\,\mathrm{K}$, and $M_{\mathrm{MCC}} = 1.2\,M_{\odot}$. The solid lines represent total planet mass, the dashed lines accumulated gas mass, and the dot–dashed lines accumulated solid mass.

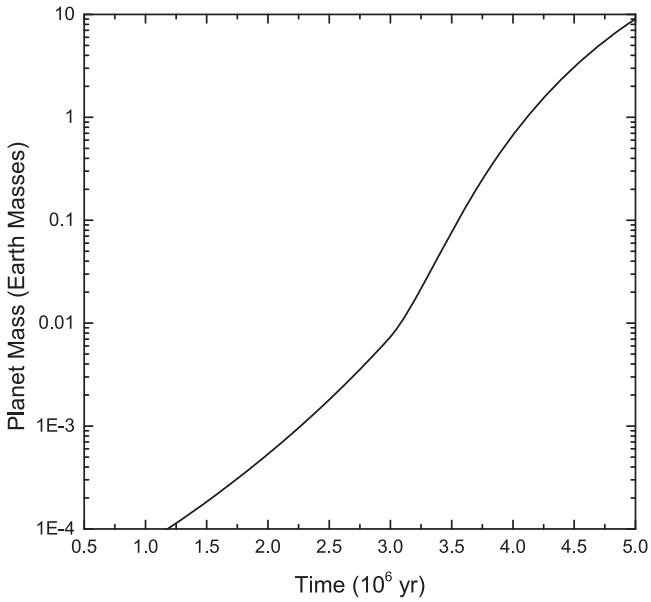

Figure 3. Time evolution of planetary mass at 39.5 au in the non-photoevaporating disk with $\omega = 1.0 \times 10^{-14}\,\mathrm{s}^{-1}$, $T_{\mathrm{MCC}} = 15\,\mathrm{K}$, and $M_{\mathrm{MCC}} = 1.2\,M_{\odot}$. The solid lines represent total planet mass, the dashed lines accumulated gas mass, and the dot–dashed lines accumulated solid mass.

the disk are high. As a result, the growth rate of the protoplanet is high. Runaway gas accretion is triggered early in the evolution of the disk. Before the disk dissipates, the planet has opened a deep gap around it. The evolutionary feature of the planet mass is characterized by the "gap-limiting" case (Tanigawa & Ikoma 2007). Since the gap width is wider than the gas accretion width (see Tanigawa & Ikoma 2007, and Figure 4 in this study), the gas accretion rate of the giant planet is very low and the planet mass almost does not change with time when the deep gap is opened. The giant planet formed in this case is the most massive (Xiao & Jin 2015). The final mass of the giant planet is mainly determined by the gap opening conditions (e.g., Kley 1999; Lubow et al. 1999; Ida & Lin 2004). Tanigawa & Ikoma (2007) estimate that the final mass, $M_{\mathrm{final,gap}}$, is proportional to $\nu/(a^2\Omega)$. Since $\nu = \alpha c_s h = \alpha c_s^2/\Omega \propto \alpha T/\Omega$, $M_{\mathrm{final,gap}} \propto \alpha T a$, where T is the disk temperature. In our disk model, $T \propto a^{-\gamma}$ with $\gamma \sim 1$ at $5 \sim 20$ au and the final mass is proportional to α (Xiao & Jin 2015). Our model show that when the planet opens a deep gap, the disk is gravitationally stable and the viscosity is low. The final mass of the planet located at 13.1 au is $\sim$1.40 M_{J}.

In Figure 2, the planet is located at 28.6 au. Since the gas surface density of the protoplanetary disk decreases with increasing R (Jin & Sui 2010), the growth rate of the protoplanet decreases. The trigger of the runaway gas accretion of the planet is delayed. Although a gap is opened, the gas accretion width exceeds the gap width and the protoplanet can still accrete gas from the disk. The evolutionary feature of the giant planet mass is characterized by the "diffusion-limiting" case (Tanigawa & Ikoma 2007). When the protoplanet can efficiently accrete the gas from the disk, the gas surface density is relatively low. The gas supply of the disk limits the gas accretion of the planet. In this case, the final mass of the planet located at 28.6 au is $\sim$0.46 M_{J}.

In Figure 3, the planet is located at 39.5 au. At the large radius of the disk, the amount of solids and gases is very small. The growth rate of the protoplanet is very low. The planet cannot accrete enough mass to trigger runaway gas accretion. As a result, it can only accrete a small amount of gas from the disk. As shown in Figure 3, the final mass of the planet located at 39.5 au is only $\sim$8.95 $M_{\oplus}$.

3.2. Gap Structures in the Non-photoevaporating Disk

The global viscous evolution of the non-photoevaporating disk is simulated by the diffusion equation, Equation (1), in which $\dot{\Sigma}_{\mathrm{w}}(R)$ is not included. The local properties of the disk near the forming planets are represented by Equation (25), which describes the equilibrium profile of the gas surface density around the planet (Tanigawa & Ikoma 2007).

Figure 4(a) shows the gas surface density profile of the disk at 0.64 Myr. During the early evolution of the disk, the masses of the planets in the disk are very low. Their gravities are too weak to affect the gas surface density of the disk. The disk evolution is derived by the viscosities due to MHD turbulence and hydrodynamic processes. The gas in the inner disk is accreted onto the central star and the gas in the outer disk expands outward.

Figure 4(b) shows the gas surface density profile of the disk at 2.56 Myr. At this time, the gas giant at 13.1 au has reached its final mass. It is massive enough to open a wide gap in the disk. However, the planet at 28.6 au is just beginning to accrete gas efficiently. Figure 2 shows that its mass is about 0.05 M_{J}. It can only open a narrow gap in the disk. The planet at 39.5 au is too small to open a gap in the disk.

Figure 4(c) shows the gas surface density profile of the disk at 5.00 Myr. Since the mass of the planet at 13.1 au rarely changes (see Figure 1), the width of the gap opened by the planet also does not changed. The planet at 28.6 au has grown to $\sim$0.46 M_{J}. The width of the gap opened by it expands but is still narrower than that at 13.1 au. The growth rate of the planet at 39.5 au is very low, and so it is still too small to open a gap.

Xiao & Jin (2015) have also shown that the formation region of giant planets is $<$30 au, which is consistent with most

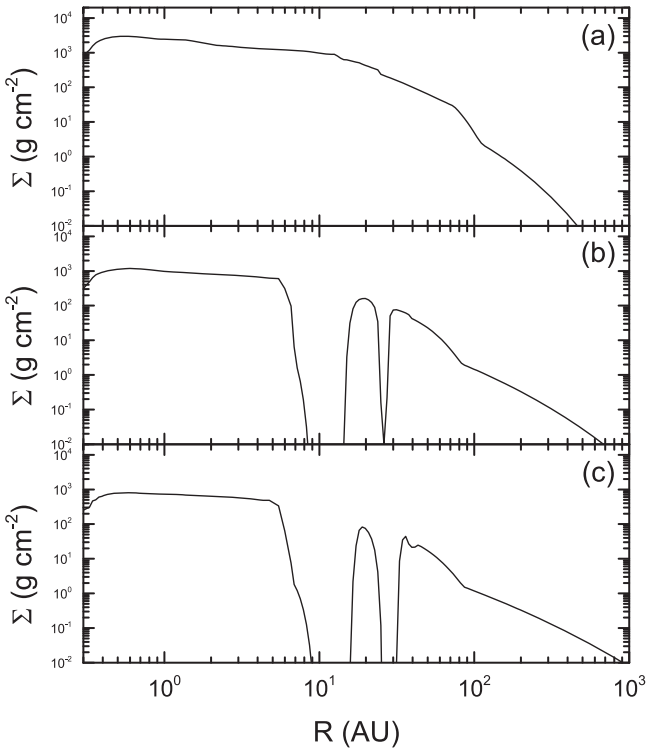

Figure 4. Gas surface density profiles of the non-photoevaporating disk with $\omega = 1.0 \times 10^{-14}$ s^{-1}, $T_{\rm MCC} = 15$ K, and $M_{\rm MCC} = 1.2\,M_{\odot}$ at (a) 0.64 Myr, (b) 2.56 Myr, and (c) 5.00 Myr.

studies of giant planet formation using the core accretion model (e.g., Pollack et al. 1996; Ida & Lin 2004; Mordasini et al. 2009; Alibert et al. 2013). Therefore, it is very difficult to open gaps by giant planets in the outer region of the disk when considering the process of giant planet formation.

3.3. Planet Formation in the Photoevaporating Disk

In the photoevaporating disk, the surface density decreases more efficiently (e.g., Alexander et al. 2014; Espaillat et al. 2014). As a result, the core accretion rate of the protoplanet declines and the trigger of the runaway gas accretion for the giant planet is delayed.

In Figure 5, the planet is located at 13.1 au. Although runaway gas accretion is delayed compared to the case shown in Figure 1, the protoplanet still has enough time to become sufficiently massive to open a deep gap. The evolutionary feature of its mass is also characterized by the "gap-limiting" case. Since the final mass of this planet is mainly determined by α, as explained in Section 3.1, this value is almost the same as that shown in Figure 1. The final mass of the planet located at 13.1 au is $\sim$1.40 $M_{\rm J}$.

In Figure 6, the planet is located at 28.6 au. The runaway gas accretion is also delayed compared to the case shown in Figure 2. However, the evolutionary feature of its mass is characterized by the "diffusion-limiting" case. The gas accretion rate of the planet is determined by the gas supply of the disk. Since photoevaporation makes Σ decrease efficiently, the Σ in the photoevaporating disk at any time will be lower than that in the non-photoevaporating disk at the same time. Therefore, the planet mass at 3.00 Myr shown in Figure 6 is relatively small with $\sim$0.14 $M_{\rm J}$ compared to that shown in Figure 2. Moreover, the efficient decrease of Σ due to photoevaporation also results in the decline of the disk lifetime (e.g., Armitage et al. 2003; Gorti et al. 2009; Ribas et al. 2015). As a result, the final mass of the planet shown in Figure 6 is much lower than that shown in Figure 2 because of the shorter gas accretion timescale.

In Figure 7, the planet is located at 39.5 au. Photoevaporation also limits disk expansion. So, Σ in the outer region of the photoevaporating disk is lower than that of the non-photoevaporating disk. In the outer region of the disk, the growth rate of the planet is low and the final mass of the planet in Figure 7 is lower than that in Figure 3.

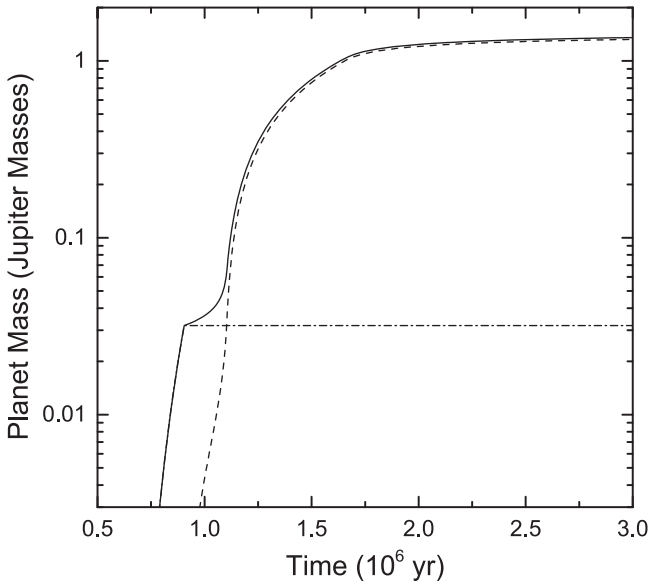

Figure 5. Time evolution of planetary mass at 13.1 au in the photoevaporating disk with $\omega = 1.0 \times 10^{-14}$ s^{-1}, $T_{\rm MCC} = 15$ K, and $M_{\rm MCC} = 1.2\,M_{\odot}$. The solid lines represent total planet mass, the dashed lines accumulated gas mass, and the dot–dashed lines accumulated solid mass.

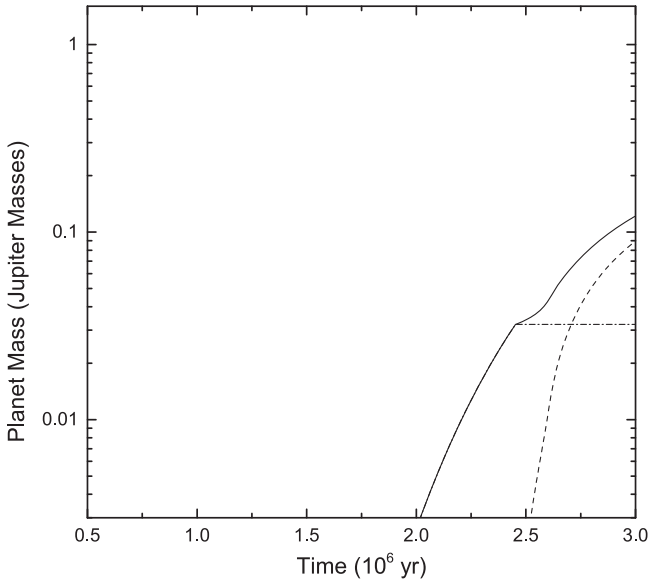

Figure 6. Time evolution of planetary mass at 28.6 au in the photoevaporating disk with $\omega = 1.0 \times 10^{-14}$ s^{-1}, $T_{\rm MCC} = 15$ K, and $M_{\rm MCC} = 1.2\,M_{\odot}$. The solid lines represent total planet mass, the dashed lines accumulated gas mass, and the dot–dashed lines accumulated solid mass.

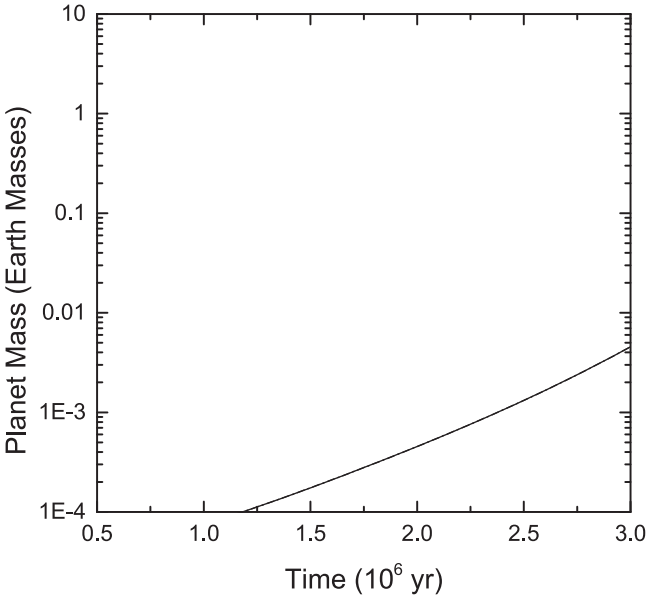

Figure 7. Time evolution of planetary mass at 39.5 au in the photoevaporating disk with $\omega = 1.0 \times 10^{-14}$ s^{-1}, $T_{\rm MCC} = 15$ K, and $M_{\rm MCC} = 1.2\,M_\odot$. The solid lines represent total planet mass, the dashed lines accumulated gas mass, and the dot–dashed lines accumulated solid mass.

3.4. Gap Structures in the Photoevaporating Disk

The global evolution of the photoevaporating disk is dominated by viscosity and photoevaporation. Figure 8 show that the mass loss due to photoevaporation results in a lower surface density profile and smaller size of the disk (expansion of the disk is suppressed). The lifetime of the photoevaporating disk is about 3 Myr, which is much shorter than that of the non-photoevaporating disk (>5 Myr).

Figure 8(a) shows the gas surface density profile of the disk at 0.64 Myr. In the early evolution of the disk, the masses of planets in the disk are too low, and so their gravities cannot affect the gas surface density profile of the disk.

Figure 8(b) shows the gas surface density profile of the disk at 2.56 Myr. At this time, the gas giant at 13.1 au has also reached its final mass as discussed in Section 3.2. It is massive enough to open a wide gap in the disk. Kanagawa et al. (2016) obtain an empirical formula of the gap width for the giant planet:

$$\frac{\Delta_{\rm gap}}{R} = 0.41\left(\frac{M}{M_*}\right)^{1/2}\left(\frac{h}{R}\right)^{-3/4}\alpha^{-1/4}. \quad (29)$$

According to Equation (24) in Jin & Sui (2010), $h/R \propto M_*^{-1/2}$. We find that $\Delta_{\rm gap} \propto M^{1/2}M_*^{-1/8}$. Since mass loss due to photoevaporation causes the central star mass to be relatively lower in the photoevaporating disk, the width of the gap opened by the planet at 13.1 au is wider than that in the non-photoevaporating disk. The planet at 28.6 au just begins to accrete gas efficiently. Figure 6 shows that its mass is about 0.04 $M_{\rm J}$. It can only open a narrow gap in the disk and the gap width is comparable to that in Figure 4(b) at 28.6 au because of the relatively low mass of the planet and the central star mass. Although the planet at 39.5 au is too small to influence the surface density profile of the disk, a gap is opened at about 80 au because the disk surface density at the radius drops more steeply than the photoevaporation rate (Bae et al. 2013).

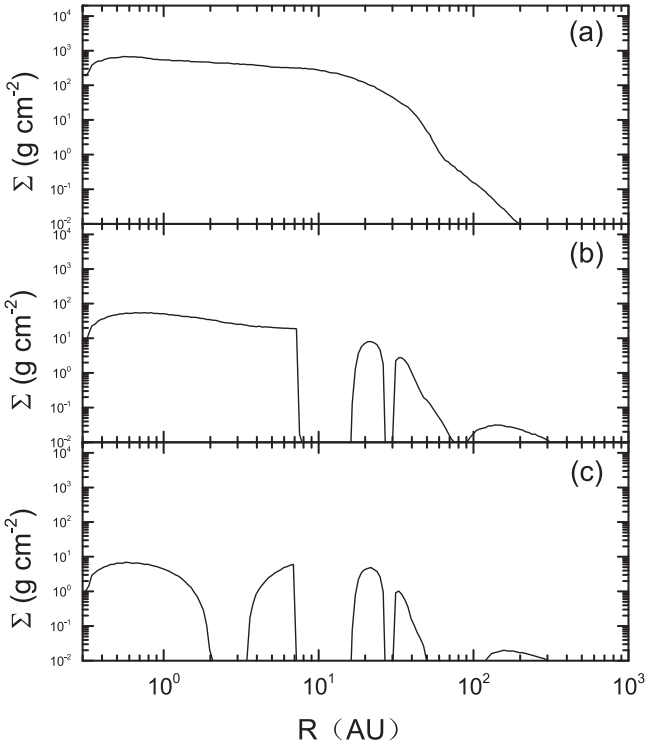

Figure 8. Gas surface density profiles of the photoevaporating disk with $\omega = 1.0 \times 10^{-14}$ s^{-1}, $T_{\rm MCC} = 15$ K, and $M_{\rm MCC} = 1.2\,M_\odot$ at (a) 0.64 Myr, (b) 2.43 Myr, and (c) 2.56 Myr.

Figure 8(c) shows the gas surface density profile of the disk at 2.56 Myr. The widths of the gaps opened by planets does not change. According to Equation (29), we calculate the widths of the two gaps. The gap at 13.1 au is about 9.47 au, which is consistent with the results of Kanagawa et al. (2016). The gap at 28.6 au is about 5.29 au, which is lower than the results of Kanagawa et al. (2016) because the planet in the gap is smaller. The outermost gap opened by photoevaporation expands because the disk globally depletes through the accretion of gas giants and photoevaporation. Due to this gas depletion, the surface density in the inner disk is lower. Numerical simulation results from Bae et al. (2013) show that the X-ray photoevaporation rate reaches the maximum value at 1–3 au. So a gap is opened at ∼2 au under the action of accretion and photoevaporation (Bae et al. 2013; Rosotti et al. 2015).

4. LIMITATIONS

Our disk model is axisymmetric, and so we cannot simulate accretion by non-axisymmetric instabilities. The accretion rates may be underestimated in some cases (e.g., Hawley 1987; Li et al. 2001; Meheut et al. 2012).

In this paper, the photoevaporation model is valid for disks around isolated stars. Therefore, a disk around a low-mass star may be dispersed by all three kinds of radiation: EUV, FUV, and X-ray (Armitage 2011). Photoevaporation driven by EUV is well understood due to the simple physics in this case (Alexander et al. 2014). The analytic mass-loss rate of EUV photoevaporation is in good agreement with that calculated by numerical models (e.g., Hollenbach et al. 1994; Alexander et al. 2006). However, the mass-loss rate of EUV

photoevaporation is relatively low. Calculations show that an EUV photoevaporating disk may last for $\gtrsim 10^7$ yr, which is much longer than the observed disk lifetimes (Alexander et al. 2006; Gorti et al. 2009). We consider that EUV photoevaporation cannot significantly affect the final mass of giant planets. Therefore, we ignore the EUV photoevaporation effect in this study. Gorti & Hollenbach (2009) show that FUV and X-ray photoevaporation produce a significant mass-loss rate, and the estimated disk lifetimes are comparable to the observed disk lifetimes. For FUV photoevaporation, the mass-loss rate is highly dependent on the thermal structure of the disk, which is still not fully understood (Armitage 2011; Alexander et al. 2014). So we adopt X-ray irradiation as the primary photoevaporation source. This simplification is still able to demonstrate the influence of photoevaporation on the properties of gas giant planets that formed in situ. According to Owen et al. (2012), our model is applicable when the X-ray luminosity is relatively strong if photoevaporation is thought to be the dominant dissipation mechanism for disks.

MRI is considered to be the most promising mechanism driving angular-momentum transport in protoplanetary disks (Balbus & Hawley 1991; Brandenburg et al. 1995; Hawley et al. 1995; Balbus et al. 1996; Balbus & Hawley 1998). However, protoplanetary disks are cold, dense, and, therefore, poorly ionized. The low level of ionization tends to decouple the disk gas from magnetic fields, which generates non-ideal MHD effects: Ohmic dissipation, ambipolar diffusion (AD), and the Hall effect (e.g., Armitage 2011; Turner et al. 2014). These effects quench MRI in different ways: Ohmic dissipation originates from collisions between electrons and neutrals, AD from collisions between ions and neutrals, and the Hall effect from drift between electrons and ions (Fleming et al. 2000; Sano & Stone 2002; Bai & Stone 2011). Ohmic dissipation operates in high-density regions with weak field, AD dominates in highly ionized and low-density regions, and the Hall effect lies in between (Fleming & Stone 2003; Bai & Stone 2011; Bai 2014). So far, the effect of Ohmic dissipation has been best studied. Investigations show the layered accretion in the inner disk, where the midplane region is "dead" due to low ionization while the surface layer is "active" due to sufficient ionization (Gammie 1996; Jin 1996; Fleming et al. 2000; Fleming & Stone 2003; Turner et al. 2007; Ilgner & Nelson 2008; Oishi & Mac Low 2009; Okuzumi & Hirose 2011). Recent works that take into account both Ohmic dissipation and AD show that AD may render the surface layer and portions of the outer disk inactive (Bai & Stone 2011; Landry et al. 2013; Kalyaan et al. 2015). Bai & Stone (2013) find that MRI is completely suppressed in the inner disk and a strong magnetocentrifugal wind is launched. Three-dimensional simulations that include all three non-ideal MHD effects are also performed (Bai 2014, 2015; Lesur et al. 2014; Simon et al. 2015). In the inner disk, the influence of the Hall effect on midplane angular-momentum transport depends on the orientation of the vertical magnetic field with the disk rotation axis. When the field is aligned with the axis, the enhanced Maxwell stress promotes angular-momentum transport. When the field is anti-aligned with the axis, the midplane remains quiescent. In the outer disk, the Hall effect has little influence on the disk turbulence. Although the inclusion of AD and the Hall effect substantially changes the level of turbulence in the protoplanetary disks, the feature that the viscosity is low in the inner disk and high in the outer disk is still valid. In this study, we assume that gas giant planets form in situ via the core accretion scenario, which implies that their formation locations are always in the low-viscosity region. Since in this study we focus on the relation between photoevaporation and planet formation and gap opening by planets in the disk, we adopt Ohmic dissipation to represent the non-ideal MHD effects on the MRI. We consider that this simplification has little influence on our main calculation results.

In this study, we also do not consider the formation of planetesimals. However, calculations have shown that the low-viscosity region in the disk is crucial to planetesimal formation (e.g., Bai & Stone 2010; Okuzumi & Hirose 2012; Drążkowska et al. 2013; Simon et al. 2016). It is worth expanding our study to investigate the influence of all three non-ideal MHD effects on the formation and evolution of planetesimals, and eventually on the properties of planets.

5. CONCLUSION

In this paper, we study giant planet formation in photoevaporating disks with long-term evolution. Our calculations show that mass loss due to photoevaporation results in a lower surface density profile and the suppression of the disk expansion. As a result, the disk lifetime is significantly shortened. The core accretion rate of the protoplanet declines and the trigger of runaway gas accretion for the giant planet is delayed under the action of photoevaporation. We find that the final mass of the giant planet characterized by the "gap-limiting" case is not influenced by photoevaporation because the protoplanet has enough time to become massive to open a deep gap and the final mass is mainly determined by α. However, the final mass of the giant planet characterized by the "diffusion-limiting" case is significantly influenced by photoevaporation. The gas accretion rate of the planet is determined by the gas supply of the disk. Since photoevaporation makes Σ decrease efficiently, Σ in the photoevaporating disk at a time is lower than that in the non-photoevaporating disk at the same time and the disk lifetime is shortened significantly. As a result, the final mass of the planet in the photoevaporating disk is much lower than that in the non-photoevaporating disk.

We also study the gas structures in the photoevaporating disk. Considering the formation process of giant planets, we suggest that the locations of gaps opened by giant planets are within 30–40 au and the gap width in the "gap-limiting" case is wider than that in the "diffusion-limiting" case. We also find that the gaps in the photoevaporating disk are wider than those in the non-photoevaporating disk. Our calculations show that a gap may be opened at a large radius of the disk if photoevaporation is thought to be the dominant dissipation mechanism for disks. We finally suggest that a gap may also be opened at 1–3 au under the actions of photoevaporative dissipation and gas accretion of the outer giant planets.

We are grateful to the anonymous referee for constructive and fruitful comments that helped us improve our paper significantly. This research has been supported in part by National Natural Science Foundation of China (NSFC) grants 11373047, 11073009, 10873006, 11373019, and 10573007.

REFERENCES

Adachi, I., Hayashi, C., & Nakazawa, K. 1976, PThPh, 56, 1756
Akiyama, E., Muto, T., Kusakabe, N., et al. 2015, ApJL, 802, L17
Akiyama, E., Hasegawa, Y., Hayashi, M., & Iguchi, S. 2016, ApJ, 818, 158

Alexander, R. D., Clarke, C. J., & Pringle, J. E. 2006, MNRAS, 369, 216
Alexander, R., Pascucci, I., Andrews, S., Armitage, P., & Cieza, L. 2014, in Protostars and Planets VI, ed. H. Beuther et al. (Tucson, AZ: Univ. Arizona Press), 475
Alibert, Y., Carron, F., Fortier, A., et al. 2013, A&A, 558, A109
ALMA Partnership, Brogan, C. L., Pérez, L. M., et al. 2015, ApJL, 808, L3
Armitage, P. J. 2011, ARA&A, 49, 195
Armitage, P. J., Clarke, C. J., & Palla, F. 2003, MNRAS, 342, 1139
Bae, J., Hartmann, L., Zhu, Z., & Gammie, C. 2013, ApJ, 774, 57
Bai, X.-N. 2014, ApJ, 791, 137
Bai, X.-N. 2015, ApJ, 798, 84
Bai, X.-N., & Stone, J. M. 2010, ApJ, 722, 1437
Bai, X.-N., & Stone, J. M. 2011, ApJ, 736, 144
Bai, X.-N., & Stone, J. M. 2013, ApJ, 769, 76
Balbus, S. A., & Hawley, J. F. 1991, ApJ, 376, 214
Balbus, S. A., & Hawley, J. F. 1998, RvMP, 70, 1
Balbus, S. A., Hawley, J. F., & Stone, J. M. 1996, ApJ, 467, 76
Benz, W., & Asphaug, E. 1999, Icar, 142, 5
Brandenburg, A., Nordlund, A., Stein, R. F., & Torkelsson, U. 1995, ApJ, 446, 741
Caselli, P., Benson, P. J., Myers, P. C., & Tafalla, M. 2002, ApJ, 572, 238
Cassen, P., & Moosman, A. 1981, Icar, 48, 353
Chambers, J. E. 2006a, ApJL, 652, L133
Chambers, J. E. 2006b, Icar, 180, 496
Dipierro, G., Price, D., Laibe, G., et al. 2015, MNRAS, 453, L73
Dong, R., Zhu, Z., & Whitney, B. 2015, ApJ, 809, 93
Drążkowska, J., Windmark, F., & Dullemond, C. P. 2013, A&A, 556, A37
Dubrulle, B. 1993, Icar, 106, 59
Ercolano, B., Clarke, C. J., & Drake, J. J. 2009, ApJ, 699, 1639
Espaillat, C., Muzerolle, J., Najita, J., et al. 2014, in Protostars and Planets VI, ed. H. Beuther et al. (Tucson, AZ: Univ. Arizona Press), 497
Fleming, T., & Stone, J. M. 2003, ApJ, 585, 908
Fleming, T. P., Stone, J. M., & Hawley, J. F. 2000, ApJ, 530, 464
Font, A. S., McCarthy, I. G., Johnstone, D., & Ballantyne, D. R. 2004, ApJ, 607, 890
Gammie, C. F. 1996, ApJ, 457, 355
Goldreich, P., & Tremaine, S. 1980, ApJ, 241, 425
Goodman, A. A., Benson, P. J., Fuller, G. A., & Myers, P. C. 1993, ApJ, 406, 528
Gorti, U., & Hollenbach, D. 2009, ApJ, 690, 1539
Gorti, U., Dullemond, C. P., & Hollenbach, D. 2009, ApJ, 705, 1237
Guilloteau, S., Dutrey, A., Piétu, V., & Boehler, Y. 2011, A&A, 529, A105
Hasegawa, Y., & Pudritz, R. E. 2011, MNRAS, 417, 1236
Hawley, J. F. 1987, MNRAS, 225, 677
Hawley, J. F., Gammie, C. F., & Balbus, S. A. 1995, ApJ, 440, 742
Ho, P. 2016, Natur, 530, 169
Hollenbach, D., Johnstone, D., Lizano, S., & Shu, F. 1994, ApJ, 428, 654
Hsi-Wei, Y., Hauyu Baobab, L., Pin-Gao, G., et al. 2016, ApJL, 820, L25
Ida, S., & Lin, D. N. C. 2004, ApJ, 604, 388
Ida, S., & Makino, J. 1993, Icar, 106, 210
Ikoma, M., Nakazawa, K., & Emori, H. 2000, ApJ, 537, 1013
Ilgner, M., & Nelson, R. P. 2008, A&A, 483, 815
Isella, A., Pérez, L. M., Carpenter, J. M., et al. 2013, ApJ, 775, 30
Jijina, J., Myers, P. C., & Adams, F. C. 1999, ApJS, 125, 161
Jin, L. 1996, ApJ, 457, 798
Jin, L., & Sui, N. 2010, ApJ, 710, 1179
Jin, S., Li, S., Isella, A., Li, H., & Ji, J. 2016, ApJ, 818, 76
Kalyaan, A., Desch, S. J., & Monga, N. 2015, ApJ, 815, 112
Kanagawa, K. D., Muto, T., Tanaka, H., et al. 2016, PASJ, 68, 43 (http://pasj.oxfordjournals.org/content/68/3/43)
Klahr, H. H., & Bodenheimer, P. 2003, ApJ, 582, 869
Kley, W. 1999, MNRAS, 303, 696
Kokubo, E., & Ida, S. 1998, Icar, 131, 171
Kokubo, E., & Ida, S. 2002, ApJ, 581, 666
Kratter, K. M., & Lodato, G. 2016, arXiv:1603.01280
Kratter, K. M., Matzner, C. D., & Krumholz, M. R. 2008, ApJ, 681, 375
Kwon, W., Looney, L. W., & Mundy, L. G. 2011, ApJ, 741, 3
Landry, R., Dodson-Robinson, S. E., Turner, N. J., & Abram, G. 2013, ApJ, 771, 80
Laughlin, G., & Bodenheimer, P. 1994, ApJ, 436, 335
Laughlin, G., & Rozyczka, M. 1996, ApJ, 456, 279
Laughlin, G., Korchagin, V., & Adams, F. C. 1997, ApJ, 477, 410
Laughlin, G., Korchagin, V., & Adams, F. C. 1998, ApJ, 504, 945
Lesur, G., Kunz, M. W., & Fromang, S. 2014, A&A, 566, A56
Li, H., Colgate, S. A., Wendroff, B., & Liska, R. 2001, ApJ, 551, 874
Lin, D. N. C., & Papaloizou, J. 1979, MNRAS, 186, 799
Lin, D. N. C., & Papaloizou, J. C. B. 1993, in Protostars and Planets III, ed. E. H. Levy & J. I. Lunine (Tucson, AZ: Univ. Arizona Press), 749
Lubow, S. H., Seibert, M., & Artymowicz, P. 1999, ApJ, 526, 1001
Masset, F. S., & Papaloizou, J. C. B. 2003, ApJ, 588, 494
Meheut, H., Meliani, Z., Varniere, P., & Benz, W. 2012, A&A, 545, A134
Miguel, Y., & Brunini, A. 2008, MNRAS, 387, 463
Miguel, Y., Guilera, O. M., & Brunini, A. 2011, MNRAS, 417, 314
Mordasini, C., Alibert, Y., Benz, W., & Naef, D. 2009, A&A, 501, 1161
Morishima, R. 2012, MNRAS, 420, 2851
Nakamoto, T., & Nakagawa, Y. 1994, ApJ, 421, 640
Nayakshin, S. 2015, MNRAS, 454, 64
Ogihara, M., Morbidelli, A., & Guillot, T. 2015, A&A, 584, L1
Oishi, J. S., & Mac Low, M.-M. 2009, ApJ, 704, 1239
Okuzumi, S., & Hirose, S. 2011, ApJ, 742, 65
Okuzumi, S., & Hirose, S. 2012, ApJL, 753, L8
Owen, J. E., Clarke, C. J., & Ercolano, B. 2012, MNRAS, 422, 1880
Owen, J. E., Ercolano, B., & Clarke, C. J. 2011, MNRAS, 412, 13
Owen, J. E., Ercolano, B., Clarke, C. J., & Alexander, R. D. 2010, MNRAS, 401, 1415
Paardekooper, S.-J., & Papaloizou, J. C. B. 2009, MNRAS, 394, 2283
Pepliński, A., Artymowicz, P., & Mellema, G. 2008, MNRAS, 386, 179
Picogna, G., & Kley, W. 2015, A&A, 584, A110
Pollack, J. B., Hubickyj, O., Bodenheimer, P., et al. 1996, Icar, 124, 62
Ribas, Á, Bouy, H., & Merín, B. 2015, A&A, 576, A52
Rice, K., Lopez, E., Forgan, D., & Biller, B. 2015, MNRAS, 454, 1940
Robitaille, T. P., Whitney, B. A., Indebetouw, R., & Wood, K. 2007, ApJS, 169, 328
Rosotti, G. P., Ercolano, B., & Owen, J. E. 2015, MNRAS, 454, 2173
Sano, T., & Stone, J. M. 2002, ApJ, 570, 314
Shakura, N. I., & Sunyaev, R. A. 1973, A&A, 24, 337
Shu, F. H. 1977, ApJ, 214, 488
Simon, J. B., Armitage, P. J., Li, R., & Youdin, A. N. 2016, ApJ, 822, 55
Simon, J. B., Lesur, G., Kunz, M. W., & Armitage, P. J. 2015, MNRAS, 454, 1117
Tamayo, D., Triaud, A. H. M. J., Menou, K., & Rein, H. 2015, ApJ, 805, 100
Tanigawa, T., & Ikoma, M. 2007, ApJ, 667, 557
Tanigawa, T., & Watanabe, S.-I. 2002, ApJ, 580, 506
Thommes, E. W., Duncan, M. J., & Levison, H. F. 2003, Icar, 161, 431
Toomre, A. 1964, ApJ, 139, 1217
Turner, N. J., Fromang, S., Gammie, C., et al. 2014, in Protostars and Planets VI, ed. H. Beuther et al. (Tucson, AZ: Univ. Arizona Press), 475
Turner, N. J., Sano, T., & Dziourkevitch, N. 2007, ApJ, 659, 729
van der Marel, N., van Dishoeck, E. F., Bruderer, S., et al. 2016, A&A, 585, A58
Williams, J. P., & Cieza, L. A. 2011, ARA&A, 49, 67
Xiao, L., & Jin, L. 2015, ApJ, 802, 79
Xiao, L., & Li, M. 2016, ApJ, submitted
Yang, H., Li, Z.-Y., Looney, L., & Stephens, I. 2016, MNRAS, 456, 2794
Zhang, K., Blake, G. A., & Bergin, E. A. 2015, ApJL, 806, L7